A Practical Visual Servo Control for an Unmanned Aerial Vehicle

Nicolas Guenard, Tarek Hamel, Robert Mahony

A Practical Visual Servo Control for an Unmanned Aerial Vehicle

N. GUENARD†, T. HAMEL‡, and R. MAHONY◇

***Abstract*— An image-based visual servo control is presented for an Unmanned aerial vehicle (UAV) capable of stationary or quasi-stationary flight with the camera mounted on board the vehicle. The target considered consists of a finite set of stationary and disjoint points lying in a plane. Control of the position and orientation dynamics are decoupled using a visual error based on spherical centroid data, along with estimations of the linear velocity and the gravitational inertial direction extracted from image features and an embedded IMU. The visual error used compensates for poor conditioning of the image Jacobian matrix by introducing a non-homogeneous gain term adapted to the visual sensitivity of the error measurements. A nonlinear controller, that ensures exponential convergence of the system considered, is derived for the full dynamics of the system using control Lyapunov function design techniques. Experimental results on a quad-rotor UAV, developed in the French Atomic Energy Commission (CEA), demonstrate the robustness and performance of the proposed control strategy.**

Keywords: Image based visual servo (IBVS), Aerial Robotic Vehicle, Under-actuated systems, Experiments.

I. INTRODUCTION

Visual servo algorithms have been extensively developed in the robotics field over the last ten years [11], [30]. Visual servo systems may be divided into two main classes [24]; *pose-based visual servo* (PBVS) control or *image-based visual servo* (IBVS) control. Position-based visual servo control (PBVS) involves reconstruction of the target pose with respect to the robot and results in a Cartesian motion planning problem. This approach requires an accurate 3D model of the target, is sensitive to camera calibration errors, and displays a tendency for image features to leave the camera field of view during the task evolution. Image-based visual servo control (IBVS) treats the problem as one of controlling features in the image plan, such that moving features to a goal configuration implicitly results in the task being accomplished [11]. Feature errors are mapped to actuator inputs via the inverse of an image Jacobian matrix. There are a wide range of features that have been considered, including points, lines, circles and image moments. Different features lead to different closed-loop responses and there has been important research into optimal selection of features and partitioned control where some degrees of freedom are controlled visually and others by a second sensor modality [19], [5]. IBVS avoids many of the robustness and calibration problems associated with PBVS, however, it has its own problems [6]. Foremost in the classical approach is a requirement to estimate the depth of each feature point in the visual data. Various solutions have been investigated, including; estimation via partial pose estimation [24], adaptive control [28], and estimation of the image Jacobian using quasi Newton technics [29]. More recently, there has been considerable interest in hybrid control methods whereby translational and rotational control are treated separately [24], [10], [8], [27]. Most existing IBVS approaches were developed for serial-link robotic manipulators [18]. For this kind of robot there are low-level joint controllers that compensate for system dynamics and position control, such as visual servo control, is undertaken at the level of the system kinematics [11]. There are very few integrated IBVS control designs for fully dynamic system models [34], [3] and even fewer that deal with under-actuated dynamic models such as Unmanned Aerial Vehicles [26], [14]. The key challenge in applying classical visual servo control to a dynamic system model lies in the highly coupled form of the image Jacobian. Much of the existing work in visual servo control of aerial robots (and particularly autonomous helicopters) have used *pose-based visual servo* methodology [1], [31], [25] that avoids the image Jacobian formulation. Prior work by the authors [14] proposed a theoretical IBVS control design for a class of under actuated-dynamics, and uses an image based visual feature augmented with an inertial direction, obtained from a partial attitude pose-estimation algorithm. In [15], a fully image based visual servo control design for dynamic systems associated with UAV systems capable of hover fight, is derived. Both control schemes assume that the translational velocity of the system is measured directly. In [22], an image-based visual servo (IBVS) control for a fully dynamic system is designed for a translational motion of a rigid body. The image features considered are a first-order un-normalised spherical moment for position stabilisation and optic flow for velocity. Direct implementation of the control strategies proposed in [14], [15], [22] have been found to have poor sensitivity and conditioning when implemented directly on an experimental vehicle.

In this paper, the practical implementation of an image-based visual servo control (IBVS) for a UAV, capable of stationary or quasi-stationary flight, is presented. The model considered is that of an 'eye-in-hand' type configuration, where the camera is attached to the airframe of the UAV. The approach taken is based on recent work by the authors [14] for which the dynamics of the image features have certain passivity-like properties. A new visual error term is considered that improves the conditioning of the image Jacobian. The initial analysis is undertaken for the kinematic response of the

†is with CEA/LIST Fontenay-aux-roses, France Email: guenardn@zoe.cea.fr

‡is with I3S, UNSA-CNRS, 2000 route des Lucioles-Les algorithmes, 06903 Sophia Antipolis, France (phone: +33 (0) 4 92 94 27 55; fax: +33 (0) 4 92 94 28 98; email: thamel@i3s.unice.fr)

◇ is with Department of Engineering, Australian National University, ACT, 0200, Australia. Robert.Mahony@anu.edu.au

Fig. 1. The X4-flyer UAV

system, the normal visual servo framework, and shows that the resulting image Jacobian is well conditioned. Following this, a non-linear controller integrating the linear and rotational dynamics is developed using a structured control Lyapunov function for exponential stabilization of the full dynamics of the UAV. The vehicle considered is equipped with an Inertial Measurement Unit (IMU) and an explicit complementary filter is used to provide filtered estimates of attitude [16] and angular velocity for the vehicle. An estimate of translational velocity is derived from a nonlinear filter that fuses IMU and visual data [7]. Experimental results are obtained on a quad-rotor UAV system, developed within the French Atomic Energy Commission (CEA), capable of stationary and quasi-stationary flight. The closed-loop visual servo control is shown to be locally exponentially stable and experimental results demonstrate the performances and robustness of the proposed control.

The paper is arranged into six sections. Following the introduction, Section II presents the fundamental equations of motion for a quad-rotor UAV. Section III presents the proposed choice of image features. Section IV provides a Kinematic control design for the translational motion. Section V extends the control to the full dynamics of the system. Section VI presents experimental results obtained on the experimental quad-rotor (Fig. 1). Finally Section VII provides some concluding remarks.

II. Dynamic Model for a hovering UAV

In this section, we present equations of motion for an UAV in quasi-stationary (or hover) flight conditions. The model used is based on those introduced in the literature to model the dynamics of helicopters [31], [13], [17]. Let $\mathcal{I} = \{E_x, E_y, E_z\}$ denote a right-hand inertial or world frame such that E_z denotes the vertical direction downwards into the earth. Let $\xi = (x, y, z)$ denote the position of the center of mass of the object in the inertial frame $\mathcal{I}$. Let $\mathcal{A} = \{E_1^a, E_2^a, E_3^a\}$ be a (right-hand) body-fixed frame centered at the center of mass and assume that it coincides with the camera frame. The orientation of the airframe is given by a rotation $R : \mathcal{A} \to \mathcal{I}$, where $R \in SO(3)$ is an orthogonal rotation matrix.

Let $V \in \mathcal{A}$ denote the linear velocity and $\Omega \in \mathcal{A}$ denote the angular velocity of the camera both expressed in the camera frame. Let m denote the mass of the rigid object and let $\mathbf{I} \in \mathbb{R}^{3\times 3}$ be the constant inertia matrix around the center of mass (expressed in the body-fixed frame $\mathcal{A}$). The dynamics of a rigid body are:

$$\dot{\xi} = RV \tag{1}$$

$$m\dot{V} = -m\Omega \times V + F \tag{2}$$

$$\dot{R} = R\text{sk}(\Omega), \tag{3}$$

$$\mathbf{I}\dot{\Omega} = -\Omega \times \mathbf{I}\Omega + \Gamma. \tag{4}$$

were the notation $\text{sk}(x)$ denotes the skew-symmetric matrix associated any vector $x \in \mathbb{R}^3$ such that for any vector $y \in \mathbb{R}^3$, $\text{sk}(x)y = x \times y$.

The exogenous force and torque are denoted F and Γ respectively. The inputs considered correspond to a typical arrangement found on a VTOL aircraft (see Sec. VI). The inputs are written as a single translational force, denoted F, along with full torque control, $\Gamma = (\Gamma_1, \Gamma_2, \Gamma_3)^T$ around around axes (E_1^a, E_2^a, E_3^a). The force F combines thrust, lift, gravity and drag components. It is convenient to separate the gravity component[1] $mgE_z = mgR^T e_3$ from the combined aerodynamic forces and assume that the aerodynamic forces are always aligned with the z-axis in the body fixed frame,

$$F := -Te_3 + mgR^T e_3, \tag{5}$$

where $T \in \mathbb{R}$ is a scalar input representing the magnitude of external force applied in direction e_3. This is a reasonable assumption for the dynamics of a UAV in quasi-stationary flight where the exogenous force is dominated by the lift force while aerodynamical drag (depending on the the square of the linear velocity) and forward thrust are negligible [32], [13], [22]. Control of the airframe is obtained by using the torque control $\Gamma = (\Gamma_1, \Gamma_2, \Gamma_3)$ to align the force (or thrust vector) $F_0 := TE_3^a = Te_3$ as required to track the goal trajectory.

III. Choice of Image Features

A. Kinematics of an image point under spherical projection

Let P be a stationary point target visible to the camera expressed in the camera frame. The image point observed by the camera is denoted p and is obtained by rescaling onto the image surface $\mathcal{S}$ of the camera. Following the approach introduced in [14] we consider a camera with a spherical image plane. Thus,

$$p = \frac{P}{|P|}. \tag{6}$$

Where $|x|$ represents the Euclidian norm of any vector $x \in \mathbb{R}^n$, $|x| = \sqrt{x^T x}$. The dynamics of an image point for a spherical camera of image surface radius unity are (see [14], [4])

$$\dot{p} = -\Omega \times p - \frac{\pi_p}{r} V, \tag{7}$$

where $r = |P|$ and $\pi_p = (I_3 - pp^T)$ is the projection $\pi_p : \mathbb{R}^3 \to T_p\mathcal{S}^2$, the tangent space of the sphere S^2 at the point $p \in \mathcal{S}^2$.

[1] Here $e_3 = (0\ 0\ 1)$ denotes the third-axis unit vector in $\mathbb{R}^3$.

B. Centroid of a target surface

Consider a point target consisting of N points $\{P_i\}$ with image points $\{p_i\}$. The centroid of a point target is defined to be

$$q_0 := \frac{\sum_{i=1}^{N} p_i}{\left|\sum_{i=1}^{N} p_i\right|} \in \mathcal{S}^2 \tag{8}$$

The centroid measures the center of mass of the *observed points* in the chosen camera geometry. The centroid depends implicitly on the camera geometry and for a different geometry (such as a camera with perspective projection) the direction of the centroid will be different.

Using centroid information is an old technique in visual servo control [2], [20], [33]. Among the advantages; in computing target centroids it is not necessary to match observed image points with desired features as would be necessary in classical image based visual servo control [18], the calculation of an image centroid is highly robust to pixel noise, and centroids are easily computed in real-time. The disadvantage of the definition (8) is that it measures only two degrees of freedom associated with the direction of centroid with respect to the body-fixed-frame axes of the camera. The un-normalised spherical centroid is defined to be

$$q := \sum_{i=1}^{N} p_i \in \mathbb{R}^3. \tag{9}$$

Intuitively, as the camera approaches the geometric center of the target points for a spherical camera geometry, the observed image points spread out around the focal point of the camera, decreasing the norm of q. In the limit, the value of q can theoretically reach zero, although for most practical systems this will not be possible while keeping the image points in the field of view of the camera. Conversely, as the camera moves away from the geometric center of the target points, the observe image points cluster together in the direction of the image. The un-normalized centroid q converges to a vector that has norm N and points towards the target. This relationship between the norm of q and the distance to the target provides a third constraint in the image based error term. It is however highly nonlinear and leads to sensitivity and conditioning problems that must be overcome in the control design.

For a point target comprising a finite number of image points, the kinematics of the image centroid are easily verified to be

$$\dot{q} = -\Omega \times q - QV, \tag{10}$$

where

$$Q = \sum_{i=1}^{i=n} \frac{\pi_{p_i}}{|P_i|} = \sum_{i=1}^{i=n} \frac{\pi_{p_i}}{r_i} \tag{11}$$

is a positive definite matrix as long as there are at least two ($N \geq 2$) visible target points (see [14] for details).

C. Image based errors

In this paper, we augment the image information with inertial information acquired from a standard inertial measurement unit (IMU) used in most small scale UAVs.

Formally, let $b \in \mathcal{I}$ denote the desired inertial direction for the visual feature. The norm of b encodes the effective depth information for the desired limit point. Define

$$q^* := R^T b \in \mathcal{A}$$

to be the desired target vector expressed in the camera fixed frame. The orientation matrix R is estimated from filtered data acquired on a strap down IMU on the vehicle. Since $q^* \in \mathcal{A}$, it inherits dynamics from the motion of the camera

$$\dot{q}^* = -\Omega \times q^*.$$

The natural image based error is the difference between the measured centroid and the target vector expressed in the camera frame

$$\delta := q - q^*. \tag{12}$$

The image error kinematics are

$$\dot{\delta} = -\Omega \times \delta - QV \tag{13}$$

To regulate the full pose of the camera using a fully-actuated kinematic system (such as a robotic manipulator) it would be necessary to introduce an additional error criterion for orientation control.

For an under-actuated dynamic system of the form Eqn's 1-4 the attitude dynamics are used to control the orientation of the vehicle thrust, that in turn provides the control of the system position dynamics. It is physically impossible to separately stabilize the attitude and position of the camera. The error criterion chosen regulates only the position of the rigid body and the orientation regulation is derived as a consequence of the system dynamics.

IV. Kinematic Control Design

In this section a Lyapunov control design is given for the kinematics of the translational motion Eq. 1 based on the visual error Eq. 13.

Define a storage function S

$$S = \frac{1}{2}|\delta|^2 \tag{14}$$

Taking the time derivative of S and substituting for Eq. 13, yields

$$\dot{S} = -\delta^T QV \tag{15}$$

Note that Eq. 15 is independent of the angular velocity Ω.

For $N \geq 2$, the matrix $Q > 0$ is known to be positive definite, and although its exact structure is not known, its maximal eigenvalue must satisfy

$$\lambda_{\max}(Q) \leq \sum_{i=1}^{i=n} \frac{1}{r_i}, \tag{16}$$

where r_i denotes the relative depth of the ith image point. Thus, a simple choice

$$V = k_\delta \delta, \quad k_\delta > 0$$

is sufficient to stabilize S for a kinematic control regime. Indeed, substituting into Eq. 15 one obtains

$$\dot{S} = -k_\delta \delta^T Q \delta$$

Since Q is a positive definite matrix, classical Lyapunov theory guarantees that δ converges exponentially to zero.

Note that the lower bound on the Jacobean Matrix norm, $||Q||$, becomes singular as the range between the camera and the target increases to infinity. The eigenvalues of the matrix Q are generally ill-conditioned

$$\lambda_{\min}(Q) << \lambda_{\max}(Q).$$

Convergence rates of the components of the error δ depend on the eigenvalues of Q. As a consequence, the natural control $V = k_\delta \delta$ leads to poor asymptotic performance of the closed-loop system.

A. Compensation of the control gain sensitivity

A number of different approaches have been proposed to compensate the poor conditioning of the Jacobian matrix Q and to improve performance of the closed-loop system [4]. In earlier work, only the kinematic model was studied and the dynamics of the system was not considered in the control design. In this paper, we propose a modification of the visual error term to improve the conditioning of the Jacobian matrix Q in the neighborhood of the set point q^*, preserving the passivity-like properties and allowing control design for the full dynamics of the system.

At the set point, the Jacobian matrix Q display two eigenvalues of comparable magnitude and one eigenvalue, associated with the direction q^*, that is an order of magnitude smaller. To deal with this ill-conditioning, two new error terms are introduced:

$$\delta_{11} = q_0^* \times q, \quad \delta_{12} = q_0^{*T}\delta, \quad q_0^* = \frac{q^*}{|q^*|} \tag{17}$$

Differentiating δ_{11} and δ_{12}, it follows that

$$\dot{\delta}_{11} = -\operatorname{sk}(\Omega)\delta_1 - \operatorname{sk}(q_0^*)QV \tag{18}$$

$$\dot{\delta}_{12} = -q_0^{*T}QV \tag{19}$$

The notation $\operatorname{sk}(x)$ denotes the skew-symmetric matrix associated with any vector $x \in \mathbb{R}^3$ such that for any vector $y \in \mathbb{R}^3$, $\operatorname{sk}(x)y = x \times y$.

Lemma 4.1: Consider the system defined by Eq. 13 and let $k_1, \lambda > 0$ be two strictly positive constants. Define

$$\delta_1 = \delta_{11} + \lambda q_0^* \delta_{12} \tag{20}$$

Assume that the image remains in the camera field of view for all time. Then, the closed loop system Eq. 13 based on the following control Eq. 21

$$V = k_1(-\operatorname{sk}(q_0^*) + \lambda q_0^* q_0^{*T})(\delta_{11} + \lambda q_0^* \delta_{12}), \tag{21}$$

exponentially stabilizes the visual error δ_1 and therefore δ.

Proof:

Define

$$S_1 = \frac{1}{2}|\delta_{11}|^2 + \lambda^2 |\delta_{12}|^2$$

It is straightforward to verify that the two components of δ_1 (δ_{11} and $q_0^*\delta_{12}$) are orthogonal and therefore:

$$S_1 = \frac{1}{2}|\delta_{11} + \lambda q_0^* \delta_{12}|^2 = \frac{1}{2}\delta_1^2$$

Deriving S_1 and substituting the control input V by its expression, yields

$$\dot{S}_1 = -k_1 \delta_1^T H \delta_1$$

where

$$H = A(q_0^*)QA(q_0^*)^T, \quad A(q_0^*) = -\operatorname{sk}(q_0^*) + \lambda q_0^* q_0^{*T} \tag{22}$$

Since Q is positive definite matrix and $A(q_0^*)$ is a non singular matrix, $H > 0$ and therefore δ_1 (respectively δ) converges exponentially to zero.

Due to the decoupling between δ_{11} and δ_{12} and the decrease of the storage function S_1 towards zero guarantee the exponential convergence of the error δ to zero. ■

Remark 4.2: The best choice of the gain λ is characterized by setting

$$H \cong I$$

where the symbol $\cong$ means "equality up to a multiplicative constant". Although, this relationship cannot be exactly assigned, it can be approximately satisfied over a large neighborhood around the desired set point and overcomes the inherent sensitivity and conditioning of the control law proposed in earlier work [14]. △

V. Control design for the full dynamics

In this section the kinematic control developed in Section IV is adapted to apply to the full under-actuated system dynamics using the back-stepping control Lyapunov function design approach.

The dynamics of the error term δ_1 (Eq. 20) may be written

$$\dot{\delta}_1 = -\operatorname{sk}(\Omega)\delta_1 - \frac{k_1}{m}H\delta_1 - \frac{k_1}{m}H\delta_2, \tag{23}$$

where δ_2 defines the difference between the desired (or virtual) kinematic controller (Eq. 21) and the true velocity

$$\delta_2 := \frac{m}{k_1}A(q_0^*)^{-T}V - \delta_1, \tag{24}$$

and will form an error term to stabilize the translational dynamics. With the above definitions one has

$$\dot{S}_1 = -\frac{k_1}{m}\delta_1^T H \delta_1 - \frac{k_1}{m}\delta_1^T H \delta_2 \tag{25}$$

It is easily verified that

$$(A(q_0^*)^{-1})^T = A(q_0^*)^{-T} = \operatorname{sk}(q_0^*) + \frac{1}{\lambda}q_0^* q_0^{*T}.$$

Deriving $A(q_0^*)^{-T}$ one obtains

$$\frac{d}{dt}(A(q_0^*)^{-T}) = -\operatorname{sk}(\Omega \times q_0^*) - \frac{1}{\lambda}\operatorname{sk}(\Omega)q_0^* q_0^{*T} + \\ + \frac{1}{\lambda}q_0^* q_0^{*T}\operatorname{sk}(\Omega) \tag{26}$$

Using the following relation:

$$\operatorname{sk}(\Omega \times q_0^*) = \operatorname{sk}(\Omega)\operatorname{sk}(q_0^*) - \operatorname{sk}(q_0^*)\operatorname{sk}(\Omega),$$

the derivative of $A(q_0^*)^{-T}$ may be rewritten as follows:

$$\begin{aligned}\frac{d}{dt}(A(q_0^*)^{-T}) &= -\text{sk}(\Omega)\text{sk}(q_0^*) + \text{sk}(q_0^*)\text{sk}(\Omega) \\ &\quad - \frac{1}{\lambda}\text{sk}(\Omega)q_0^*q_0^{*T} + \frac{1}{\lambda}q_0^*q_0^{*T}\text{sk}(\Omega) \\ &= -\text{sk}(\Omega)A(q)^{-T} + A(q)^{-T}\text{sk}(\Omega) \qquad (27)\end{aligned}$$

Deriving δ_2 and recalling Eqn's 2, 23 and 27, one obtains

$$\dot{\delta}_2 = -\text{sk}(\Omega)\delta_2 + \frac{k_1}{m}H\delta_1 + \frac{k_1}{m}H\delta_2 + \frac{1}{k_1}A(q_0^*)^{-T}F \quad (28)$$

Let S_2 be a second storage function associated with the translational dynamics

$$S_2 = \frac{1}{2}|\delta_1|^2 + \frac{1}{2}|\delta_2|^2. \qquad (29)$$

Taking the time derivative of S_2 it follows that

$$\dot{S}_2 = -\frac{k_1}{m}\delta_1^T H\delta_1 + \frac{k_1}{m}\delta_2^T H\delta_2 + \frac{1}{k_1}\delta_2^T A(q_0^*)^{-T}F. \quad (30)$$

The positive definite matrix $H = A(q_0^*)QA(q_0^*)^T$ is not exactly known, however, for a suitable choice of λ it will be well conditioned with known bounds on eigenvalues in a large neighborhood of the desired set point. Thus, choosing

$$F := -\frac{k_1^2k_2}{m}A(q_0^*)^T\delta_2, \qquad (31)$$

where $k_2 > \lambda_{\max}(H) = \max\{\lambda_{\max}(Q), \lambda^2\lambda_{\min}(Q)\}$, is sufficient to stabilize the translational dynamics. Since the rigid body system considered is under-actuated, the force input F cannot be directly assigned. The proposed control algorithm continues the backstepping procedure by using the above definition as a virtual input. A virtual differentiation $\dot{T}$ of thrust is introduced in the following development to ensure decoupling between translational and rotational dynamics as shown in the sequel (see Eq. 37).

Set

$$F^v := -\frac{k_1^2k_2}{m}\delta_2. \qquad (32)$$

A new error term δ_3 is defined to measure the scaled difference between the virtual and the true force inputs

$$\delta_3 := \frac{m}{k_1^2k_2}A(q_0^*)^{-T}F + \delta_2. \qquad (33)$$

The derivative of δ_2 (Eq. 28) becomes

$$\dot{\delta}_2 = -\text{sk}(\Omega)\delta_2 + \frac{k_1}{m}H\delta_1 - \frac{k_1}{m}(k_2I_3 - H)\delta_2 + \frac{k_1}{m}k_2\delta_3, \qquad (34)$$

and the derivative of the second storage function is now

$$\dot{S}_2 = -\frac{k_1}{m}\delta_1^T H\delta_1 - \frac{k_1}{m}\delta_2^T(k_2I_3 - H)\delta_2 + \frac{k_1}{m}k_2\delta_2^T\delta_3. \quad (35)$$

Deriving δ_3 and recalling Eq. 28, yields

$$\begin{aligned}\dot{\delta}_3 = &-\text{sk}(\Omega)\delta_3 + \frac{k_1}{m}H\delta_1 - \frac{k_1}{m}(k_2I_3 - H)\delta_2 + \frac{k_1}{m}k_2\delta_3 \\ &+ \frac{m}{k_1^2k_2}A(q_0^*)^{-T}\left(\dot{F} + \text{sk}(\Omega)F\right) \qquad (36)\end{aligned}$$

Recalling Eq. 5, the full vectorial term $\left(\dot{F} + \text{sk}(\Omega)F\right)$ is explicitly given by

$$\left(\dot{F} + \text{sk}(\Omega)F\right) = \begin{pmatrix} 0 & T & 0 \\ -T & 0 & 0 \\ 0 & 0 & 1 \end{pmatrix}\begin{pmatrix} \Omega_1 \\ \Omega_2 \\ \dot{T} \end{pmatrix} \qquad (37)$$

The goal of the paper is to control the full system dynamics Eqn's 1-4. In practice, the IMU on board a flying vehicle provides high bandwidth low noise measurements of angular velocity Ω of the vehicle. This allows us to apply a high gain control loop around the angular dynamics (Eq. 4) and use the angular velocity Ω as an input to the remainder of the system dynamics Eqn's 1-3. Control of Eqn's 1-3 relies on much lower bandwidth visual feedback and occurs at a much lower bandwidth than the angular velocity control. In fact, only the first two components of the angular velocity Ω_1 and Ω_2 are required in the visual servo control loop, along with the set point for the dynamic extension of the thrust $\dot{T}$.

Proposition 5.1: Consider the system dynamics Eqn's 1-3 with inputs $(\Omega_1, \Omega_2, \dot{T})$. Let δ_1 be defined by Eq. 20 and δ_2, δ_3 be defined by Eq. 24 and Eq. 33 respectively. Choose $(\Omega_1, \Omega_2, \dot{T})$ according to Eq. 37 such that

$$\frac{m}{k_1^2k_2}\left(\dot{F} + \text{sk}(\Omega)F\right) := -\frac{(k_1k_2 + k_3)}{m}A(q_0^*)^T\delta_3 \qquad (38)$$

for $k_1, k_3 > 0$ and $k_2 > \lambda_{\max}(H)$. Then δ_1 is locally exponentially stable to zero and the attitude direction R^Te_3 is locally exponentially stable to e_3.

Proof: Let $\mathcal{L}$ be a Lyapunov candidate function defined by

$$\mathcal{L} = \frac{1}{2}|\delta_1|^2 + \frac{1}{2}|\delta_2|^2 + \frac{1}{2}|\delta_3|^2 = S_2 + \frac{1}{2}|\delta_3|^2 \qquad (39)$$

Taking the derivative of $\mathcal{L}$, and recalling 35 and 36, one obtains

$$\begin{aligned}\dot{\mathcal{L}} = &-\frac{k_1}{m}\delta_1^T H\delta_1 - \frac{k_1}{m}\delta_2^T(k_2I_3 - H)\delta_2 + \frac{k_2}{m}\delta_2^T\delta_3 \\ &\frac{k_1}{m}\delta_3^T H\delta_1 - \frac{k_1}{m}\delta_3^T(k_2I_3 - H)\delta_2 + \frac{k_1}{m}k_2\delta_3^T\delta_3 \\ &+ \frac{m}{k_1^2k_2}\delta_3^T A(q_0^*)^{-T}\left(\dot{F} + \text{sk}(\Omega)F\right)\end{aligned}$$

Introducing the expression Eq. 38 in the Lyapunov function derivative, one obtains

$$\begin{aligned}\dot{\mathcal{L}} = &-\frac{k_1}{m}\delta_1^T H\delta_1 - \frac{k_1}{m}\delta_2^T(k_2I_3 - H)\delta_2 + \\ &\frac{k_1}{m}\delta_3^T H\delta_1 - \frac{k_1}{m}\delta_3^T(k_2I_3 - H)\delta_2 - \frac{k_3}{m}\delta_3^T\delta_3\end{aligned}$$

Completing the square three times to dominate the cross terms, it may be verified that the choice of control gains given in the theorem ensures that the right-hand side is negative definite in all the error signals δ_i, $i = 1, \ldots, 3$. Classical Lyapunov theory ensures exponential convergence of $\delta_i \to 0$.

If the position and linear velocity are regulated then the total external force must be zero, $F = 0$. Recalling Eq. 5 one has

$$R^Te_3 = e_3, \quad T = mg. \qquad (40)$$

■

Note that the error term δ_3 does not determine the full attitude of the system considered. Only pitch and roll components of the attitude are regulated by the error δ_3 while the yaw rotation around the thrust direction is independent of the error criteria. In practice, it is desirable to stabilise the yaw of the vehicle to avoid unwanted second order dynamic effects and provide a stabile platform for sensor systems. Different solutions may be used to stabilize the freedom of yaw rotation in the attitude dynamics. An additional visual error is proposed in Hamel *et al.* [14], however, this leads to significant additional complexity in the mathematical development. To avoid complexity, a simple damping term

$$\Gamma_3 = -k_4 \Omega_3, \qquad k_4 > 0,$$

can be used to stop unwanted rotation without specifying a specific yaw set point. The solution adopted in the experimental Section VI is a hybrid control where the position, pitch and roll of the vehicle are controlled autonomously, while the yaw is manually servo-controlled using the operator joystick.

VI. Experimental results

In this section, the control algorithm presented in Proposition 5.1 is implemented on a quad-rotor, made by the CEA, (Fig. 1).

A quad-rotor is a vertical take off and landing vehicle ideally suited for stationary and quasi stationary flight. The vehicle consists of four individual fans fixed to a rigid cross frame. An idealized dynamic model of the quad-rotor [17], [1] is given by the rigid body equations (Eqn's 1-4) along with the external force and torque inputs (cf. Fig. 2)

$$T = T_{rr} + T_{rl} + T_{fr} + T_{fl}, \tag{41}$$
$$\Gamma_1 = d(T_{fr} + T_{fl} - T_{rr} - T_{rl}), \tag{42}$$
$$\Gamma_2 = d(T_{rl} + T_{fl} - T_{rr} - T_{fr}), \tag{43}$$
$$\begin{aligned}\Gamma_3 &= Q(T_{fr}) + Q(T_{rl}) + Q(T_{fl}) + Q(T_{rr}) \\ &= \kappa\left(T_{fr} + T_{rl} - T_{fl} - T_{rr}\right). \end{aligned} \tag{44}$$

The individual thrust of each motor is denoted $T_{(.)}$, while κ is the proportional constant giving the induced couple due to air resistance for each rotor and d denotes the distance of each rotor from the centre of mass of the quad-rotor.

The control set point for T is obtained by integration of the third component of Eq. 38, while the control torques Γ_1 and Γ_2 are obtained via a high gain stabilisation of the first two components of Eq. 4 to the control set points given by the first two components of Eq. 38. The final torque component Γ_3 is independently determined via high gain feedback control to a set point Ω_3 derived from the joystick.

The parameters used for the dynamic model have been identified as follows: $m = 0.55$ kg, $I = \text{diag}(0.009, 0.009, 0.018)$ kg.m^2, $d = 0.23$m, $\kappa = 0.018$m and $g = 9.8$m.s^{-2}.

A. Prototype description

The CEA's quad-rotor is equipped with a set of four electronic boards (Fig. 3b) designed by the CEA. Vibration absorbent material was placed between the electronic boards and the airframe to minimise sensor noise in the MEMS sensor

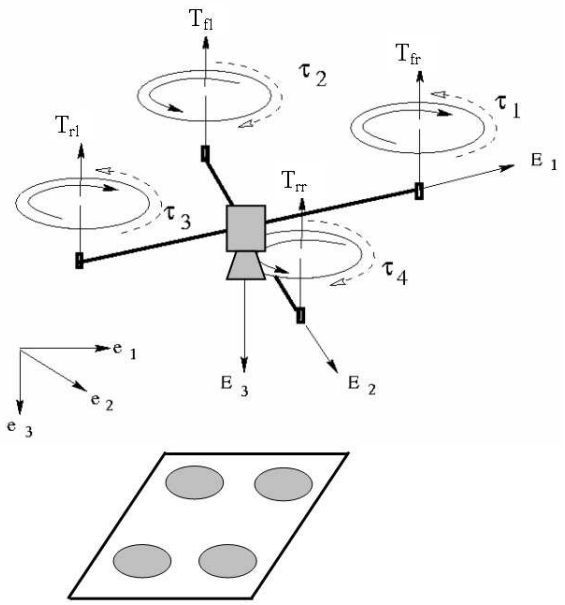

Fig. 2. The force and torque inputs for an X4-flyer.

components. Each electronic board includes a micro-controller and has a particular function. The first board integrates the motor controllers which regulate the rotation speed of the four propellers. The second board integrates an Inertial Measurement Unit (IMU), developed by the CEA, consisting of 3 low cost MEMS accelerometers, 3 angular rate sensors and 2 magnetometers. The explicit complementary filter [16] is used to estimate the attitude vector (pitch and roll) and gyros bias from IMU data. On the third board, a Digital Signal Processing (DSP), running at 150 MIPS, is embedded and performs the control algorithm and filtering computations. The final board provides a serial wireless communication between the operator's joystick and the vehicle. An embedded camera (Fig. 3a) with a field of view of 120° is mounted pointing down, and transmits video to a ground station (PC) via a wireless analogical link at 2.4GHz. Finally, a Lithium-Polymer battery provides nearly 10 minutes of flight time. The images sent by

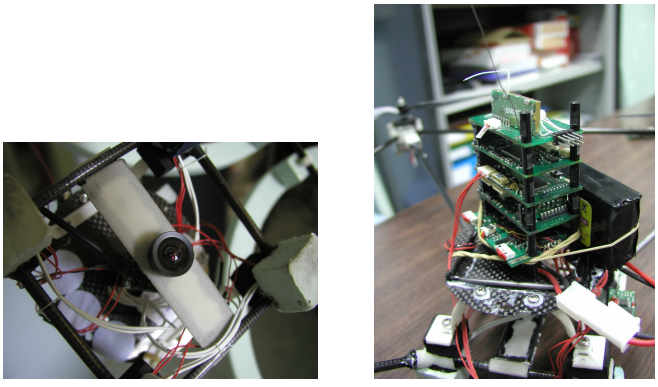

(a) (b)

Fig. 3. The embedded camera (a) and the set of electronic boards (b).

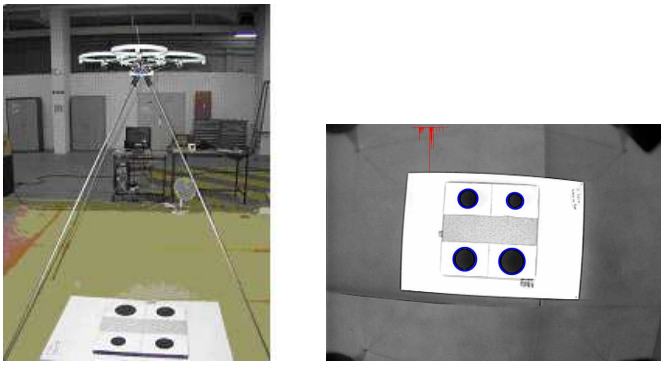

(a) (b)

Fig. 4. Initialization of the algorithm (a) ant the target view from the camera (b).

the embedded camera are received by the ground station at a frequency of 15Hz. In parallel, the quad-rotor sends the inertial data to the ground station at 9Hz. The data is processed by the ground station PC and incorporated into the control algorithm. The visual servo control algorithm is computed in the ground station PC and provides desired orientation velocities and a desired thrust rate. These control set points are transmitted to the drone where the high gain control of motor torque is embedded on the DSP running at 166Hz. This high gain control ensures stability of the vehicle despite the presence of significant latency incurred in the reception and processing of inertial data and visual features and the transmission of control demand.

B. Experiments

The target considered consists of the four black marks on the vertices of a stationary planar square (Fig. 4b). A standard computer vision segmentation algorithm extracts the marks from the background and computes the central moment of each mark. The central moments are transformed into unit-norm spherical image plane representation using the camera calibration matrix provided by the manufacturer. The four image points obtained in this manner are summed to compute the unnormalised spherical centroid q (Eq. 9). The characteristics of experimental camera insures that the observed target remains visible if the quad-rotor remains in cone of angle $\approx 45^\circ$ around the observed target and has at most $\approx 5^\circ$ inclination. This generates a workspace of diameter approximately 1.5m around the center of the target at an altitude of 1.4m.

The desired image feature b^* is chosen such that the camera set point is located 1.4m above the target

$$b^* \simeq \begin{pmatrix} 0 \\ 0 \\ 3.9 \end{pmatrix} \tag{45}$$

Figure 4a shows the unmanned aerial vehicle mounted at the set point during the process of acquiring the set point image for the image error.

1) Initialization: To implement the control algorithm it is necessary to estimate the parameter λ that is integral in improving the conditioning of the Jacobian matrix Q around the desired position. The set point for the experiment was set at $(x, y, z) \simeq (0, 0, 1.4)$m (Fig. 4a) leading to a Jacobian matrix

$$Q^* \simeq \begin{pmatrix} 2.35 & 0 & 0 \\ 0 & 2.36 & 0 \\ 0 & 0 & 0.056 \end{pmatrix}. \tag{46}$$

The condition number of Q^* is $\rho(Q^*) = \frac{\lambda_{\max}(Q^*}{\lambda_{\min}(Q^*)} \simeq 42.14$. The asymptotic convergence rates of the proposed algorithm are given by the eigenvalues of $H = A(q_0^*)Q^*A(q_0^*)^T$. For the experimental configuration considered one has (see Eq. 22)

$$A(q_0^*) = \begin{pmatrix} 0 & 1 & 0 \\ -1 & 0 & 0 \\ 0 & 0 & \lambda \end{pmatrix}. \tag{47}$$

Choosing $\lambda = 6.44$ one obtains

$$A(q_0^*)Q^*A(q_0^*)^T = 2.35 \begin{pmatrix} 1 & 0 & 0 \\ 0 & 1 & 0 \\ 0 & 0 & 1 \end{pmatrix}. \tag{48}$$

Since $H = A(q_0^*)QA(q_0^*)^T \approx A(q_0^*)Q^*A(q_0^*)^T$ in the vicinity of the set point it is expected that the overall system performance will be acceptable.

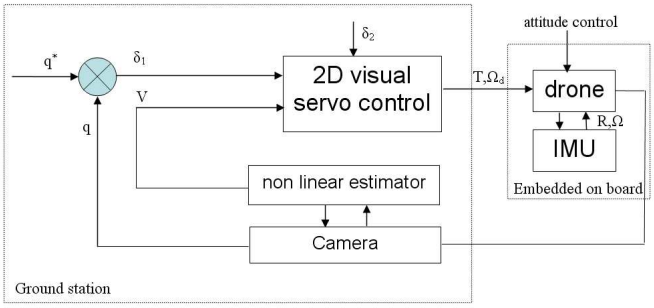

Fig. 5. Schematic block diagram of estimation and control loops.

2) Results: During the experiments, the yaw velocity (Ω_3) was controlled via the joystick. Yaw velocity does not affect the proposed control scheme (Eq. 37) and the convergence of the closed-loop system is independent of the operator input. The drone is flown under manual control into the neighbourhood of the target to ensure the target marks are visible before the control algorithm is engaged. An estimate of the initial position is $(x_0, y_0, z_0) \simeq (0.7, -0.8, 2)$m.

The exponential convergence of the visual error δ_1 is clearly visible in Figure 6. The separate convergence of the error terms δ_{11} and δ_{12} are shown in Figures 7 and 8. Figure 9 shows the evolution of the centroid vector, q, and Figure 10 shows the convergence of thrust direction Re_3 to e_3. Figure 11 shows the evolution of target points in the image space. Figure 12 shows the position evolution of the quad-rotor in the Cartesian space as obtained from the full pose estimation algorithm that

was run separately in parallel to the control algorithm[2]. The closed-loop performance of the system maintains an error of approximately 10cm around the desired position (Fig. 12). The authors believe that the most significant source of error is due to aerodynamic disturbances that can be considered as a load disturbance to the system. Any rotor craft creates vortices at the tips of the rotor plane when in hover. These vortices grow in size and strength, and then become unstable and get sucked through the rotor, causing a momentary loss of lift, before a new vortex begins to grow. Interestingly, this effect is worst in stationary hover conditions as translation through the air causes the proto-vortices to be washed through the rotor before they have built up energy. Other sources of error in the closed-loop system may come from system modelling and transmissions delays. Despite the errors, experiments show that they regulation error remains bounded and smaller than 10cm around the desired position. The authors feel that the practical stability is very good with regards to experimental system considered.

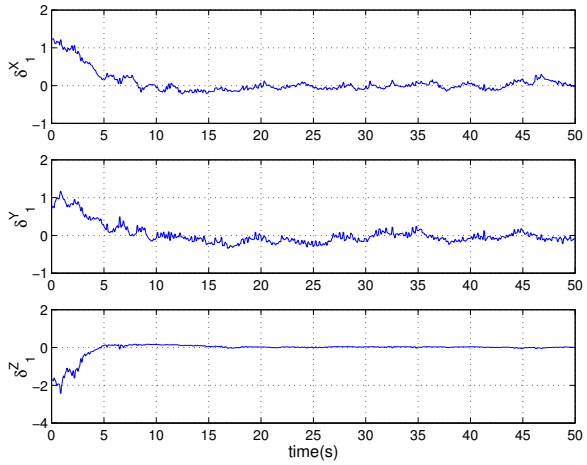

Fig. 6. Error term δ_1.

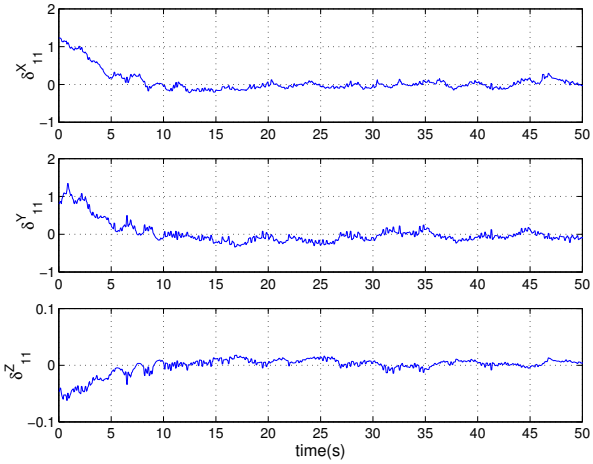

Fig. 7. Error term δ_{11}.

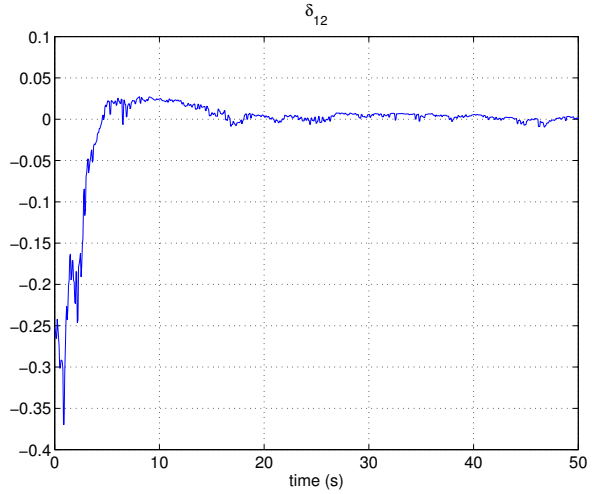

Fig. 8. Error term δ_{12}.

VII. Conclusion

In this paper we presented a visual servo control for stabilization of a quad-rotor UAV. This work is an extension of the recent theoretical work on visual servo control of under-actuated systems [14] that overcomes ill-conditioning of the Jacobian matrix. Based on the previous work [4], a new visual error is proposed that improves the conditioning of the closed-loop Jacobian matrix in the neighborhood of the desired set point. A nonlinear controller is derived, using backstepping techniques, and implemented on an experimental flying robot developed by the CEA. The experimental result show good performance and robustness of the proposed control strategy.

Acknowledgment

This work has been supported by the French company "WANY Robotics www.wanyrobotics.com" within the frame-work of a CEA-WANY Ph.D grant and a CNRS PICS grant (France-Australia).

[2]Note that the only place where the full pose estimates are used is to plot Figure 12, although the pose estimation algorithm is used to generate estimate of linear velocity used in the control algorithm.

References

[1] Altug, E., Ostrowski, J., & Mahony, Control of a quadrotor helicopter using visual feedback. In *Proceedings of the IEEE international conference on robotics and automation*, ICRA2002, Vol.1, pages: 72-77.

[2] R. L. Andersson. A Robot Ping-Pong Player: Experiment in Real-Time Intelligent Control. *MIT Press*, Cambridge, MA, USA, 1988.

[3] Astolfi, A., Hsu, L., Netto, M., & Ortega, R., Two solutions to the adaptive visual servoing problem. *IEEE Transactions on Robotics and Automation*, Vol.18(3), 2002, 387-392.

[4] O. Bourquardez, R. Mahony, T. Hamel, F. Chaumette. Stability and performance of image based visual servo control using first order spherical image moments. In *IEEE/RSJ Int. Conf. on Intelligent Robots and Systems*, IROS'06, Beijing, China, October 2006, pages: 4304 - 4309.

[5] A. Castano and S. Hutchinson. Visual compliance: Task directed visual servo control. *IEEE transactions on Robotics and Automation*, Vol.10(3), pages: 334-341, June 1993.

[6] F. Chaumette. Potential problems of stability and convergence in image-based and position-based visual servoing. In *The Conference of Vision and Control*, LNCIS, No. 237, pages: 66-78, 1998.

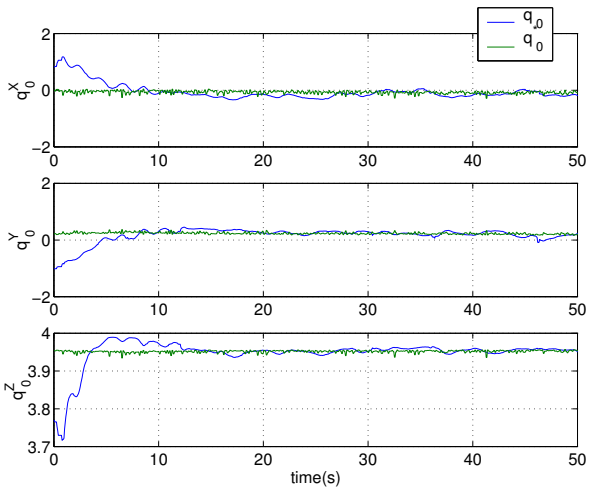

Fig. 9. Centroid evolution.

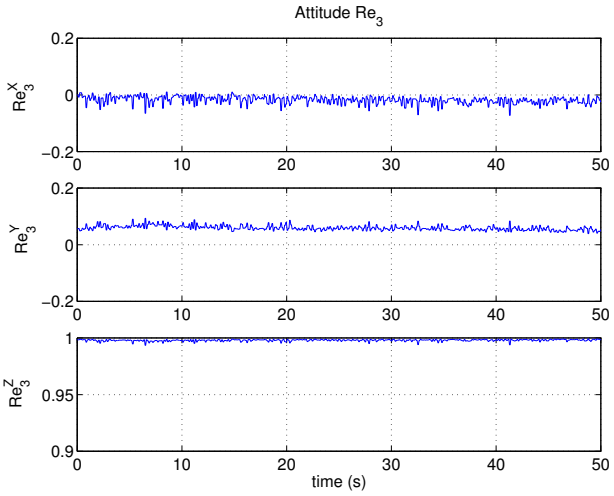

Fig. 10. **Evolution of the components of the vector Re_3.**

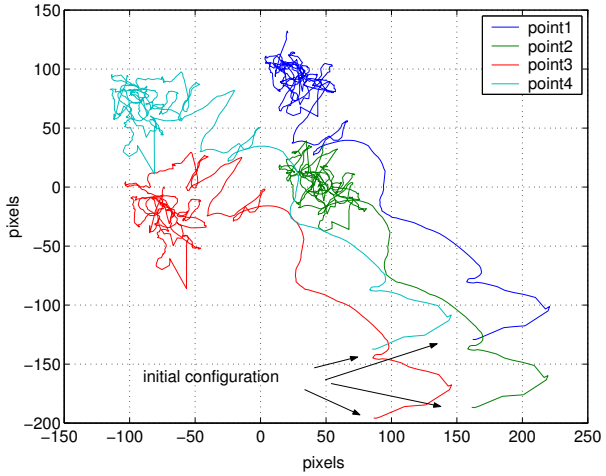

Fig. 11. Trajectory in the image plan of the four black marks.

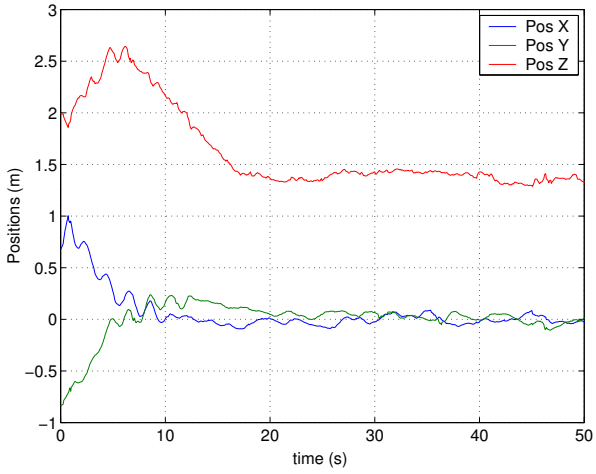

Fig. 12. 3D UAV position.

[7] Chevirond T., Hamel T., Mahony R. and Baldwin G. Robust Nonlinear Fusion of Inertial and Visual Data for position, velocity and attitude estimation of a UAV. In *IEEE Int. Conf. on Robotics and Automation*, 10-14 April 2007, Roma, Italy. IEEE-ICRA'2007, pages: 2010-2016.

[8] P. I. Corke and S. A. Hutchinson. A new partitioned approach to image-based visual servo control. In *Proceedings of the International Symposium on Robotics*, Montreal, Canada, May 2000.

[9] P. I. Corke and S. A. Hutchinson. A new hybrid image-based visual servo control scheme. In *IEEE Int. Conf. on Decision and Control*, CDC'2000, Sydnet, Australia, December 2000, pages: 2521 - 2526

[10] K. Deguchi. Optimal motion control for image-based visual servoing by decoupling translation and rotation. In *Proceedings of the International Conference on Intelligent Robots and Systems*, pages 705–711, 1998.

[11] B. Espiau, F. Chaumette, and P. Rives. A new approach to visual servoing in robotics. *IEEE Transactions on Robotics and Automation*, Vol.8(3), pages: 313-326, 1992.

[12] C. Fermuller, Y. Aloimonos. Observability of 3D motion. *International Journal of Computer Vision*, 37(1), pages: 43-64, June 2000.

[13] E. Frazzoli, M. A. Dahleh, and E. Feron. Real-time motion planning for agile autonomous vehicles. *AIAA Journal of Guidance, Control, and Dynamics*, Vol.5(1):116-129, 2002.

[14] T. Hamel and R. Mahony, Visual servoing of an under-actuated dynamic rigid-body system: An image based approach. *IEEE Transactions on Robotics and Automation*, 2002, Vol. 18(2), pages: 187-198.

[15] Hamel T. and Mahony R. Image based visual servo-control for a class of aerial robotic systems. Automatica, 2007, Vol 43, pages: 1975-1983.

[16] T. Hamel and R. Mahony. Attitude estimation on $SO(3)$ based on direct inertial measurements. In *International Conference on Robotics and Automation*, ICRA'06, Orlando, Florida, 15-19 May 2006, pages: 2170-2175.

[17] T. Hamel, R. Mahony, R. Lozano, and J. Ostrowski. Dynamic modelling and configuration stabilization for an X4-flyer. In *International Federation of Automatic Control Symposium, IFAC2002*, Barcelona, Spain, 2002.

[18] S. Hutchinson, G. Hager, and P. Cork. A tutorial on visual servo control. *IEEE Transactions on Robotics and Automation*, 12(5): 651-670, 1996.

[19] K. P. Khosla, N. Papanikolopoulos, and B. Nelson. Dynamic sensor placement using controlled active vision. In *Proceedings of IFAC 12th World Congress*, pages 9.419-422, Sydney, Australia, 1993.

[20] M. Lei and B. K. Ghosh. Visually guided robotic motion tracking. In *Proceedings of the thirteenth Annual Conference on Communication, Control and Computing*, pages 712-721, 1992.

[21] Mahony R., Corke P. and Hamel T. Dynamic image-based visual servo control using centroid and optic flow features. Journal of Dynamic Systems Measurement and Control, 130(1), january 2008.

[22] Mahony R., Hamel T. Robust trajectory tracking for a scale model autonomous helicopter. *International Journal of Non-linear and Robust Control*, Vol. 14, pages: 1035-1059, 2004.

[23] Mahony R., Hamel T. et Chaumette F. A Decoupled Image Space Approach to Visual Servo Control of a Robotic Manipulator. In *Proceedings of International Conference IEEE, Robotics and Automation*, ICRA'2002, pages: 3781-3786.

[24] E. Malis, F. Chaumette, and S. Boudet. 2-1/2-d visual servoing. *IEEE*

Transactions on Robotics and Automation, Vol.15(2): 238-250, April 1999.

[25] Metni N. and Hamel T. Visual Tracking Control of Aerial Robotic Systems with Adaptive Depth Estimation. International Journal of Control, Automation, and Systems. Vol.5, No.1, pages: 51-60, 2007.

[26] L. Mejias, S. Saripalli, G.S. Sukhatme, and P. Cervera, Visual servoing for tracking features in urban areas using an autonomous helicopter, *In Journal of Field Robotics*, 2006. Vol 23. Issue 3-4, pages: 185-199.

[27] G. Morel, T. Liebezeit, J. Szewczyk, S. Boudet, and J. Pot. Explicit incoporation of 2D constraints in vision based control of robot manipulators. Volume 250 of *Lecture Notes in Control and Information Sciences*, pages: 99-108. Springer-Verlag, New York, USA, 1999. Edited by P. Corke and J. Trevelyan.

[28] N. Papanikolopoulos, P. K. Khosla, and T. Kanade. Adaptive robot visual tracking. In *Proceedings of the American Control Conference*, pages: 962-967, 1991.

[29] J. A. Piepmeier. A dynamic quasi-newton method for model independent visual servoing. *Ph.D thesis*, Georgia Institute of Technology, Atlanta, USA, July 1999.

[30] R. Pissard-Gibollet and P. Rives. Applying visual servoing techniques to control of a mobile hand-eye system. In *Proceedings of the IEEE International Conference on Robotics and Automation*, ICRA'95, pages: 166-171, Nagasaki, JAPAN, 1995.

[31] Shakernia, O., Ma, Y., Koo, T. J., & Sastry, S. Landing an unmanned air vehicle: vision based motion estimation and nonlinear control. *Asian journal of control*, Vol.1(3), pages: 128-146, 1999.

[32] H. Shim T. Koo, F. Hoffmann, and S. Sastry, A comprehensive study of control design for an autonomous helicopter, In *Proceedings of 37th Conference on Decision and Control*, Florida, USA, 1998, pages: 3653 - 3658.

[33] B. Yoshimi and P. K. Allen. Active, uncalibrated visual servoing. In *Proceedings of the IEEE International Conference on Robotics and Automation*, ICRA'94, pages: 156-161, San Diago, CA, USA, 1994.

[34] Zergeroglu, E., Dawson, D., de Queiroz, M., & Nagarkatti, S. Robust visual-servo control of robot manipulators in the presence of uncertainty. In *Proceedings of the 38th Conference on Decision and Control*, 1999, pages: 4137-4142.

Nicolas Guenard was graduated from ETACA, the French Engineering school in Automobile, Aeronautics and Aerospace in 2003. He conducted his Ph.D. research at the Laboratory of Teleoperation and Robotic, at the French Atomic Energy Commission (CEA), in Fontenay-Aux-Roses, France and received the Ph.D. degree in Sciences from Nice-Sophia Antipolis University in 2007. Since 2007, his research interests at the CEA include localization an navigation of Unmanned Aerial Vehicle.

Tarek Hamel received his Bachelor of Engineering from the University of Annaba, Algeria, in 1991. He received his PhD in Robotics in 1995 from the University of technology Compiègne (UTC), France. After two years as a research assistant at the UTC, he joined the "Centre d'Etudes de Mècanique d'Iles de France" in 1997 as an associate professor. Since 2003, he has been a Professor at the I3S UNSA-CNRS laboratory of the University of Nice-Sophia Antipolis, France. His research interests include non-linear control theory, estimation and vision-based control with applications to Unmanned Aerial Vehicles and Mobile Robots.

Robert Mahony is currently a reader in the Department of Engineering at the Australian National University. He received a PhD in 1995 (systems engineering) and a BSc in 1989 (applied mathematics and geology) both from the Australian National University. He worked as a marine seismic geophysicist and an industrial research scientist before completing a two year postdoctoral fellowship in France and a two year Logan Fellowship at Monash University in Australia. He has held his post at ANU since 2001. His research interests are in non-linear control theory with applications in robotics, geometric optimisation techniques and learning theory.